201122058A

厚生労働科学研究費補助金

障害者対策総合研究事業(身体・知的等障害分野)

体幹保持機能障害のある身体障害者に対して生体内3次元解析システムを用いた脊椎骨構築
および動態情報フィードバック型革新的体幹保持デバイスの開発に関する研究

平成２３年度　総括・分担研究報告書

研究代表者　菅本　一臣

平成24(2012)年　5月

目　　次

厚生労働科学研究費補助金（障害者対策総合研究事業（身体・知的等障害分野））
統括研究報告書

体幹保持機能障害のある身体障害者に対して生体内3次元解析システムを用いた脊椎骨構築および動態情報フィードバック型革新的体幹保持デバイスの開発に関する研究

総括研究者 菅本 一臣 大阪大学大学院医学系研究科寄附講座教授

研究要旨　ポリカーボネイト製で作成した体幹デバイスの装着前後でコンピュータソフトを用いた評価システムを用いて、側弯における脊椎変形の３次元変形評価を行い。その矯正率を詳細に評価し、その改良の指標とした。

梶浦一郎・社会福祉法人 愛徳福祉会 南大阪療育園 理事長
山崎隆治・大阪大学臨床医工学融合研究教育センター 特任准教授

A．研究目的

身体障害者に生じる体幹保持機能低下によって発症する側湾に対してポリカーボネイト製のカスタム体幹装具を作成する。その前後で脊椎変形の３次元変形評価を行い、最適の装具の作成を目指す。

B．研究方法

骨関節の構築を3次元的に解析できるシステムを開発してきたが、それを用いることにより骨関節形態を3次元的に評価することができる。今回脊椎側弯を有する身体障害者に対してポリカーボネイト製カスタム装具装着の前後でCTにて頚椎より骨盤にかけて撮影を行い、その矯正率を算出し、最適な装具開発を目指す。

（倫理面への配慮）

本研究は大学の倫理委員会にてすでに承認済みである。ただし被爆はゼロではなく、治療効果を正確に判定する目的があるとはいえ被験者に危険を及ぼす可能性があるために、インフォームドコンセントを得る必要がある。また得られたデータは個人情報として扱われるべきものであるため、そのデータ管理にはセキュリティーを十分考量する。

C．研究結果

脳性麻痺側彎症8例，特発性側彎症8例を対象とした．これを撮影したものを共同研究者の梶浦らに解析を行わせた。その結果、Cobb角度で38度から22度へ約40％の改善率がみられた。

D．考察

これまで考えられてきた以上に側弯における脊椎変形は平面的なものではなく、３次元的な変形が大きく、それを今回提案したシステムで評価することによって、最適の装具を提供できる可能性が示唆された。

E．結論

本研究では，側彎における脊柱変形を3次元形態学的について明らかにした．特に回旋変形の評価はこれによって評価が可能であり、提案のポリカーボネイト製デバイスで40％の改善が得られていることが明らかとなった。

F．健康危険情報

CTでは被爆量を通常の1/10以下でも可能であり、全脊椎を撮影しても５mSv程度である。またそれは大学の倫理委員会にてすでに承認済みである。ただし被爆はゼロではなく、治療効果を正確に判定する目的があるとはいえ被験者に危険を及ぼす可能性があるために、インフォームドコンセントを得る必要がある。

G．研究発表

1.　論文発表　In vivo three-dimensional segmental analysis of adolescent idiopathic scoliosis. Hattori T, Sakaura H, Iwasaki M, Nagamoto Y, Yoshikawa H, Sugamoto K. Eur Spine J. 2011 Oct;20(10):1745-50. Epub 2011 Jun 18.

2.　学会発表

56th Annual Meeting of the Orthopaedic Research Society Mar. New Orleans.
In vivo three-dimensional kinematics of the cervical spine during head rotation in patients with degenerative cervical spine
Nagamoto Y, Ishii T, Sakaura H, Iwasaki M, Moritomo H, Kashii M, Sugamoto K, Yoshikawa H.

H．知的財産権の出願・登録状況

1.　特許取得

特願2007－328479

2.　実用新案登録

なし

3. その他

なし

厚生労働科学研究費補助金（障害者対策総合研究事業（身体・知的等障害分野））
分担研究報告書

脳性麻痺側彎症における体幹保持破綻に伴う脊椎変形の生体内３次元解析に関する研究

研究分担者 梶浦　一郎　社会福祉法人大阪発達総合療育センター南大阪療育園理事長

研究要旨　肢体不自由児に代表されるような身体障害者において、体幹保持機能はADL上最も重要な機能のひとつである。本研究では体幹保持機能障害を有する身体障害者に対して革新的体幹保持デバイスの開発し、ADLを向上と続発する側弯などの不可逆的な脊椎変形を予防することを目的とする。また我々が開発してきた独自のシステムによりX線イメージ装置とCT装置を組み合わせて骨関節形態および動態を３次元的に解析し、身体特性データをフィードバックしながらデバイスを最適化する。

A．研究目的

身体障害者の ADL 上重要な体幹保持機能障害に対して、独自の３次元的解析を用いて骨関節形態および動態をフィードバックした革新的体幹保持デバイスを開発および最適化し、続発する側彎などの不可逆的な脊椎変形を予防する。

B．研究方法

対象は側弯を有する脳性麻痺患者30名(男性16名、女性14名)。平均年齢は14.5才。全脊椎2方向X線検査によりデバイス装着前後の側彎変形を評価した。デバイスによるADL変化については介護者アンケートを使用した。

(倫理面への配慮) CTは被爆量を通常の1/10以下、全脊椎撮影で５mSv程度である。またそれは大学の倫理委員会にてすでに承認済みである。撮影では被験者に危険を及ぼす可能性があるために、インフォームドコンセントを得る必要がある。リスクなどを口頭で説明し同意書に署名された場合のみ解析を行う。同意が得られなかった場合にはCT撮影は行わない。また得られたデータは個人情報として管理にはセキュリティーを十分考慮する。

C．研究結果

Cobb角はデバイス非着用時に平均66.4度、着用時に平均52.8度であり、デバイスによる側彎矯正は平均13.6度となった。介護者アンケートでは、84%の患者において座位機能の安定、92%で上肢機能の改善が報告された。

D．考察

装着感の良い持続可能な当該デバイスで十分な側彎変形の矯正が可能であった。座位の安定など ADL の改善を認めた。今後はこれら所見と CT 検査を基に３次元解析を進めて身体特性のフィードバックによるデバイスの最適化を進める。

E．結論

当該デバイスは脳性麻痺などによる身体障害者において良好なコンプライアンスで導入可能であった。CT 検査による３次元解析と並行して行う臨床経過および ADL に関する評価方法が確立した。

F．健康危険情報

特になし

G．研究発表

1.　論文発表　幼児期発症の側彎変形に対するDSB（愛称プレーリーくん）による治療の試み（第一報）．近畿小児整形．2011；24：1−4

2.　学会発表

Rett症候群に伴う側彎変形に対する装具(DSB)治療経過 第45回日本側彎症学会年次総会 2011年10月

H．知的財産権の出願・登録状況

1. 特許取得
   平成23年5月　「動的脊椎装具・プレーリーくん」特許取得　特許番号4747327

2. 実用新案登録
   なし

3. その他
   なし

厚生労働科学研究費補助金（障害者対策総合研究事業（身体・知的等障害分野））
分担研究報告書

医用画像に基づく３次元動態計測手法を応用した各種脊椎計測・解析に関する研究

研究分担者　山崎　隆治　大阪大学臨床医工学融合研究教育センター・特任准教授

研究要旨　前年度（平成 22 年度）では，医用画像を用いた脊椎骨に特化した新しい３次元動態計測手法の開発を行い，主に正常および変形腰椎を想定した検証実験および動態計測を実施した．本研究（平成 23 年度）では，動態計測手法をさらに拡張し，頸椎を対象として３次元動態計測・解析を試みた．本研究により脊椎を構成する各種椎骨の正確な動態を解析可能であることが確認され，全椎骨の動態情報をフィードバックさせる新しい体幹保持デバイスの開発を促進させる可能性があることが示唆された．

A．研究目的

これまでに，脊椎骨に特化した新しい３次元動態計測手法の開発を行い，特に腰椎に対して正常および変形の動き模擬した検証実験，および動態計測・解析を実施してきた．本研究では，これまでの計測手法をさらに拡張し，頸椎を対象とした３次元動態計測・解析を実現する．これにより，脊椎を構成する全ての椎骨の動態情報をフィードバックさせる新しい体幹保持デバイスの開発の可能性が開ける．

B．研究方法

頸椎（第１頸椎（C1）～第７頸椎（C7））の３次元骨形状モデルは，CT 装置を用いて取得・作成する．実際の頸椎の動きは，動画対応型フラットパネルディテクタ装置を用いて撮影し，高鮮鋭・高解像度のディジタルデータを取得する．これらの画像データから，２次元/３次元画像位置合わせ技術（画像認識技術）を用いて，全ての頸椎骨モデルの位置と姿勢を推定し，３次元的な動態を計測・解析する．今回拡張した手法には，医用画像に特有のノイズが発生した状態でも，安定した位置・姿勢推定が可能となるようロバスト統計学に基づいたアルゴリズムを導入している．

実験は，健常ボランティア 9 名に対して，X 線透視下における側方向からの前屈・後屈運動（最大屈曲から最大伸展までの運動）と左右回旋運動（最大左回旋から最大右回旋までの運動）を実施した．また同様にして，X 線透視下における前後方向からの左右回旋運動（開口位）と側屈運動を実施した．評価項目としては，C1-C2，C2-C3，C3-C4，C4-C5，C5-C6，C6-C7 間の動きを対象とした．

（倫理面への配慮）

今回拡張した計測手法を用いて，X 線撮影実験を行うにあたり，本研究機関における倫理委員会の承認を得，また被検者には検査目的の十分な説明を行って同意を得た．

C．研究結果

現在，一部（３名）の解析結果が得られているので報告する．頸部最大回旋時における C1-C2 間の回旋角度は，同方向に平均 37.3±0.3° 回旋することが認められ，回旋の大部分は C1-C2 間で行われることが確認された．また，最大回旋時の側屈カップリング運動は，C2-C3，C3-C4，C4-C5，C5-C6，C6-C7 間では同方向に側屈するのに対し，C1-C2 間では反対方向に側屈（平均 3.4±1.4°）することが確認された．

D．考察

本研究における頸椎を対象とした３次元動態解析計測手法は，安定かつ高精度な方法であり，これにより全椎骨の動態機能評価が可能であると考えられる．

E．結論

本研究により，全椎骨の動態情報をフィードバックさせる新しい体幹保持デバイスの開発を促進させる可能性があることが示唆された．

G．研究発表

1．論文発表

・Three-dimensional kinematic estimation of mobile-bearing total knee arthroplasty from x-ray fluoroscopic images, Proceedings of SPIE Medical Imaging, Vol.7962 B1-7, 2011

・3D Spine Kinematics on Riding Fitness Machines Using 2D/3D Image Registration, IFMBE Proceedings, 2012 (in press)

2．学会発表

・In vivo three-dimensional determination of normal knee kinematics from dynamic flat-panel detector images, The 11th CAOS-International, 2011, London

・Robust 3D Kinematic Estimation of Total Knee Arthroplasty From X-Ray Fluoroscopic Images, The 24th ISTA, 2011, Belgium

・脊椎外科領域における３次元画像解析の臨床応用，第 24 回バイオエンジニアリング講演会，2012 年，大阪

H．知的財産権の出願・登録状況　なし

研究報告書

研究成果の刊行に関する一覧表

書籍

著者氏名	論文タイトル名	書籍全体の編集者名	書　籍　名	出版社名	出版地	出版年	ページ

雑誌

発表者氏名	論文タイトル名	発表誌名	巻号	ページ	出版年
Hattori T, Sakaura H, Iwasaki M, Nagamoto Y, Yoshikawa H, Sugamoto K	In vivo three-dimensional segmental analysis of adolescent idiopathic scoliosis.	Eur Spine J.	20(10)	1745-50	2011
梶浦一郎、森口悠	幼児期発症の側彎変形に対するDSB(愛称プレーリーくん)による治療の試み（第一報）	近畿小児整形外科	24	29-32	2011
T. Yamazaki, et.al	Three-dimensional kinematic estimation of mobile-bearing total knee arthroplasty from x-ray fluoroscopic images	Proceedings of SPIE Medical Imaging	7962	B1-B7	2011
T. Yamazaki, et.al	3D Spine Kinematics on Riding Fitness Machines Using 2D/3D Image Registration	IFMBE Proceedings			2012 (in press)

Eur Spine J (2011) 20:1745–1750
DOI 10.1007/s00586-011-1869-4

ORIGINAL ARTICLE

In vivo three-dimensional segmental analysis of adolescent idiopathic scoliosis

Takako Hattori · Hironobu Sakaura · Motoki Iwasaki · Yukitaka Nagamoto · Hideki Yoshikawa · Kazuomi Sugamoto

Received: 9 August 2010 / Revised: 16 April 2011 / Accepted: 29 May 2011 / Published online: 18 June 2011

Abstract
Introduction An accurate assessment of three-dimensional (3D) intervertebral deviation is crucial to the better surgical correction of adolescent idiopathic scoliosis (AIS). However, a precise 3D study of intervertebral deviation has not been previously reported.
Objective The purpose of the present study is to evaluate the intervertebral coronal inclination, axial rotation and sagittal angulation of AIS using 3D bone models and a local coordinate system.
Materials and methods 3D bone models of the thoracic and lumbar spine of ten AIS patients were constructed using computed tomography. The local coordinate axis was determined semi-automatically for each vertebra. By using these local coordinates, the intervertebral deviation angles were calculated in the coronal, axial and sagittal planes and projected to subjacent local coordinates.
Result The intervertebral deformity in the coronal plane was larger near the apical region and smaller near the junctional region. Conversely, the intervertebral rotation in the axial plane was smaller near the apical region, and larger near the junctional region. Concerning the sagittal plane deformity, the constant tendency was not recognized.
Conclusion Using a local coordinate system for the vertebra of AIS, we measured the 3D intervertebral coronal, axial and sagittal deviation of the thoracolumbar spine and found that the change in the intervertebral inclination angle in the coronal plane increased toward the apical region and decreased toward the junctional region, and that the converse tendency was noted for the axial intervertebral rotational angle. This analysis provides an improved 3D guide for the surgical correction of AIS.

Keywords Idiopathic scoliosis · Three-dimensional · Intervertebral deviation · Local coordinate system

T. Hattori (✉) · Y. Nagamoto · K. Sugamoto
Division of Orthopaedic Biomaterial Science, Osaka University Graduate School of Medicine, 2-2, Yamadaoka, Suita, Osaka 565-0871, Japan
e-mail: takako-hattori@umin.ac.jp

H. Sakaura · M. Iwasaki · H. Yoshikawa
Department of Orthopaedics, Osaka University Graduate School of Medicine, 2-2, Yamadaoka, Suita, Osaka 565-0871, Japan

Introduction

Adolescent idiopathic scoliosis (AIS) is a three-dimensional (3D) deformity associated with lateral deviation in the coronal plane, thoracic hypokyphosis in the sagittal plane and rotation in the axial plane [3, 4, 25]. However, two-dimensional evaluation of AIS remains the mainstay of most studies of AIS [10, 18]. In 2008, Modi et al. [18] reported the wedging angle of both the vertebral body and intervertebral disc and correlated the apical wedging angle and the severity of the curve in 150 AIS patients using only anteroposterior radiographs in the standing position. For evaluation in the transverse plane, Kotwicki et al. [10] used only a single axial slice from a computed tomography (CT) scan at the apex to measure the rotational angle and the intravertebral deformation. The asymmetry in the shape of the vertebral body and spinal canal and rotational deformity in the axial plane in AIS patients further contribute to the inaccuracy of such assessments of the vertebral axis in the two-dimensional plane.

3D evaluation of AIS is also gaining popularity. The in vitro 3D reconstruction of cadaveric vertebrae using 3D morphometric analysis [21–23], such as vertebral wedging, pedicle width, pedicle length, pedicle height, pedicle

inclination and facet surface, is a recent example. In addition, several studies concerning 3D reconstruction of the spine using biplane radiographic images have been reported [2, 8, 9]. The method proposed by Kadoury et al. enabled 3D reconstruction from biplane radiographs. Although their studies involve 3D analysis of an in vivo model, their reconstructed bone models used anthropometric data and not patients' bones.

An accurate assessment of 3D intervertebral deviation is crucial to the better surgical correction of the deformity. Although there have been some studies regarding intervertebral deviation of AIS [5, 7, 24], no detailed 3D study using an in vivo model of AIS has been reported. Therefore, the present study aimed to develop a local coordinate system for the AIS vertebra and to evaluate the in vivo 3D intervertebral deviation in the coronal, axial and sagittal planes in order to provide guidance for its surgical correction.

Materials and methods

Patients

We examined spinal CT images from consecutive ten patients with AIS who were scheduled for corrective surgery. The patients included two males and eight females, with an age range of 12 to 19 years (mean 14.7 years) at the time of operation. Before CT imaging, anteroposterior (AP) plain radiographs were taken in the upright position. On AP radiographs, the measured mean Cobb's angles were 62.5° (range 29°–77°) at the thoracic curvature and 50.3° (range 30°–73°) at the lumbar curvature. According to King's classification [11], the curves were type I in two patients, type II in one, type III in six and type IV in one. Risser sign [15] showed grade 0 in two, grade 3 in four, and grade 4 in four patients. Nash and Moe's vertebral rotation [19] of the apex showed grade + in one, grade ++ in seven, and grade +++ in two patients.

The protocol was approved by the institutional boards of the hospital and fully informed consent was obtained from all participants.

CT image acquisition

Prior to surgery, all ten patients underwent CT scans of the entire deformed spine in the supine position. Scans were performed using a helical CT scanner (Light Speed VCT, General Electric, Maukesha, WI). The slice thickness was 0.625 mm, the tube voltage was 120 kV and the amperage was 90 mA. The data were saved in a standard DICOM (Digital Imaging and Communications in Medicine) format. The estimated radiation dose for the patients using this scanning protocol was 5.2 mSv.

Construction of 3D surface bone models

To construct the 3D bone models, we performed a segmentation procedure. Segmentation extracts bone regions and associates each region with individual bones. The anatomic structure or region of interest must be delineated and separated so that it can be viewed individually. Regions of individual bones were segmented semiautomatically using a software program for image analysis (Virtual Place-M; AZE Ltd, Tokyo, Japan). We then obtained the surface models of the vertebrae by applying 3D surface generation of the bone cortex [18, 20].

Axis configuration of local anatomic coordinate system

In order to measure the deviation in three dimensions between adjacent vertebrae, we first established the axis of the local coordinate system for each vertebra by first calculating the centroid of the vertebra automatically and designating it as the origin of the coordinate axis (Fig. 1a). Next, the planar approximation of the superior endplate was calculated using the least-squares method and we estimated a plane parallel to the superior endplate via the origin (Fig. 1b). On that plane, a line from both the centroid and the point which divided the front part of the vertebral body into half (using the least-squares method) formed the z axis (Fig. 1c), with 'anterior' as the 'positive' direction. A line perpendicular to the z axis pointing to the left formed the x axis. Finally, the y axis was defined as a line perpendicular z–x plane (Fig. 1d).

Measurement of intervertebral coronal plane deformity

The intervertebral coronal inclination between adjacent vertebrae was defined as the angle between adjacent x axes projected on the subjacent local coordinate x–y plane. From T1–T2 to L4–L5, each intervertebral coronal inclination was measured. For example, the adjacent inclination in the coronal plane of T8–T9 represented the angle between x axes of T8 and T9 projected to the x–y plane of T9 (Fig. 2). All adjacent intervertebral angles were measured automatically.

Measurement of intervertebral axial plane deformity

The intervertebral rotation in the axial plane between adjacent vertebrae was defined as the angle between adjacent z axes projected on the subjacent local coordinate z–x plane. From T1–T2 to L4–L5, each intervertebral axial rotation angle was measured. For example, the adjacent rotation in the axial plane of T8–T9 represented the angle between z axes of T8 and T9 projected to the z–x plane of

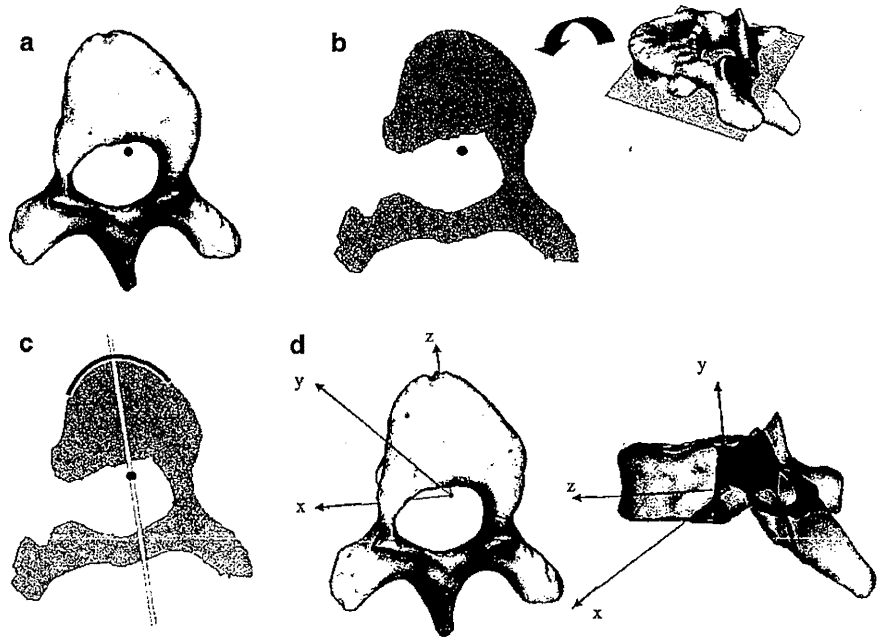

Fig. 1 The method used to establish the local coordinate system. **a** The *black sphere* is a centroid of the vertebra that is defined as the origin of the coordinate axis. **b** The cross-sectional surface of the vertebra; the planar approximation of the superior endplate was calculated using the least-squares method, and we estimated a plane parallel to the superior endplate via the origin. **c** In the cross-sectional plane, the z axis is defined as a line between the centroid and the point that divides the front portion of the vertebral body in half. **d** A line perpendicular to the z axis and pointing to the left on the plane forms the x axis. Finally, the y axis pointing cranial is defined as a line perpendicular to the z–x plane

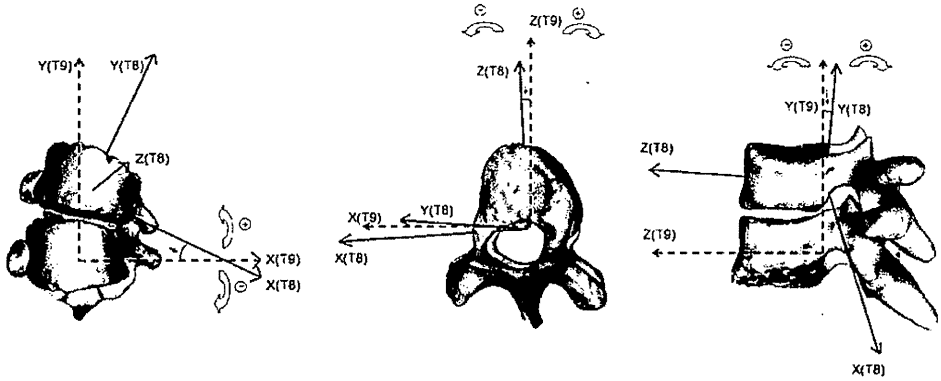

Coronal plane deformity Axial plane deformity Sagittal plane deformity

Fig. 2 The T8 and T9 bone models and each local coordinate axis. The *solid lines* present the axis of T8, and the *broken lines* present the axis of T9. *Left* the intervertebral coronal inclination. The figure faces the subjacent vertebral x–y plane; the intervertebral coronal inclination angle (*arrow*) is defined as the angle between two adjacent x axes projected on the subjacent x–y plane. *Middle* the intervertebral axial rotation. The figure faces the subjacent z–x plane; the intervertebral axial rotational angle (*arrow*) is defined as the angle between adjacent z axes projected on the subjacent z–x plane. *Right* the intervertebral sagittal angulation. The figure faces the subjacent y–z plane; the sagittal intervertebral angulation (*arrow*) is defined as the angle between adjacent y axes projected on the subjacent y–z plane

T9 (Fig. 2). All adjacent intervertebral angles were also measured automatically.

Measurement of intervertebral sagittal plane deformity

The intervertebral angulation in the sagittal plane between adjacent vertebrae was defined as the angle between adjacent y axes projected on the subjacent local coordinate y–z plane. From T1–T2 to L4–L5, each intervertebral sagittal angulation was measured. For example, the adjacent angulation in the sagittal plane of T8–T9 represented the angle between y axes of T8 and T9 projected to the y–z plane of T9 (Fig. 2). All adjacent intervertebral angles were also measured automatically.

Results

Intervertebral coronal plane deformity

The left side of Fig. 3 shows the amount of change between each intervertebral coronal inclination for all ten patients. These results indicate that the intervertebral deformity in the coronal plane was larger near the apical region and

smaller near the junctional region. The maximum intervertebral change at apical region was 20.2° (absolute value), the minimum change at junctional region was 0°. Figure 4 shows two representative cases (Case 3 and Case 10). The 3D models of both the thoracic and lumbar spine and the intervertebral angle in the coronal and axial planes are shown in Fig. 4. The x axis of the graph to the left of the bone model represents the intervertebral inclination angle in the coronal plane. The 'plus' direction of the graph means that the x axis of the suprajacent vertebra is directed in the 'plus' direction in relation to the subjacent vertebral y axis. Similarly, the minus direction of the graph means that the adjacent vertebral x axis is directed in the minus direction in relation to the y axis of the subjacent vertebra (Fig. 2).

Intervertebral axial plane deformity

The middle of Fig. 3 shows the amount of change between each intervertebral axial rotation for all patients. As the converse to the intervertebral coronal deformity, the intervertebral rotation in the axial plane was smaller near the apical region and larger near the junctional region. The maximum intervertebral change at junctional region was 12.6° (absolute value), the minimum change at apical region was 0°. The angle to the plus direction represents the amount of axial rotational change in the clockwise rotation of the suprajacent vertebra to subjacent z–x plane. On the other hand, when the suprajacent vertebral body rotates to the counterclockwise for the subjacent vertebral body, the change in the angle of the adjacent vertebral body is directed in the minus direction (Fig. 2). The amount of changes between adjacent vertebral axial rotation of two representative cases (Case 3 and Case 10) are shown in the graphs to the right of the bone models (Fig. 4).

Intervertebral sagittal plane deformity

The right side of Fig. 3 shows the amount of change between each intervertebral sagittal angulation for all the patients. Concerning the sagittal plane deformity, the constant tendency was not recognized. The 'plus' represents that the y axis of the suprajacent vertebra is directed in the minus direction in relation to the subjacent vertebral z axis. It means that the suprajacent vertebral bodies located in extension to subjacent vertebral bodies on subjacent y–z planes (Fig. 2).

Discussion

Idiopathic scoliosis is a complex spinal deformity characterized by lateral curvature of the spine associated with axial vertebral rotation. Recent 3D evaluations of the spine

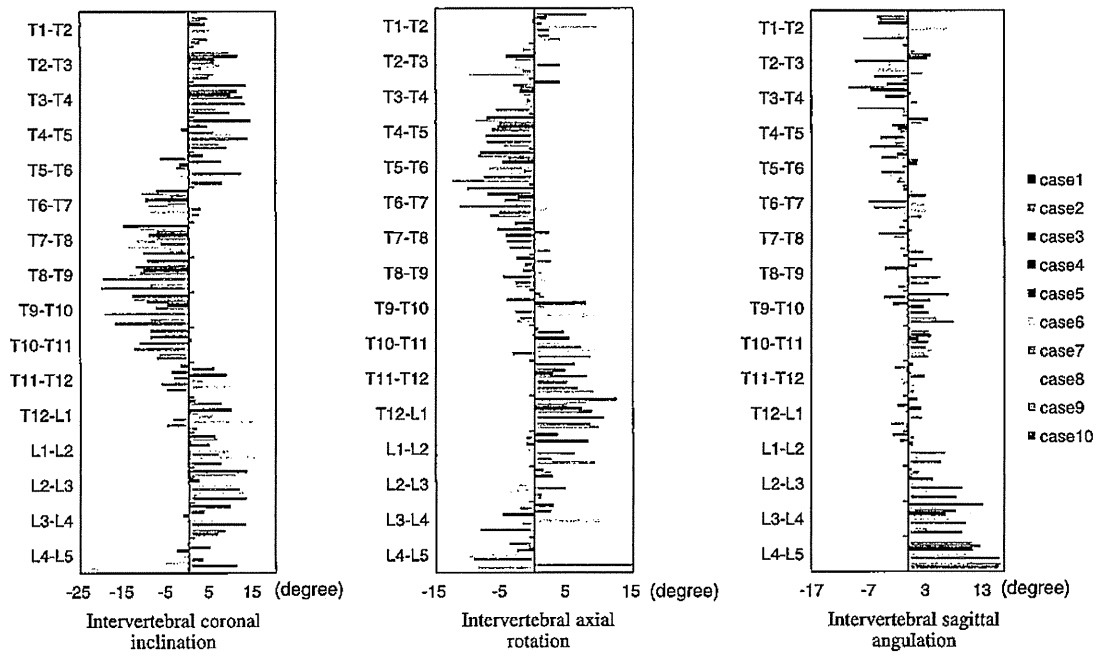

Fig. 3 The intervertebral deviation of the each adjacent vertebrae of all ten patients. The x axes show the each intervertebral deviation angles of all patients in coronal, axial and sagittal plane. The intervertebral deformity in the coronal plane was larger near the apical region and smaller near the junctional region. Conversely, the intervertebral rotation in the axial plane was smaller near the apical region, and larger near the junctional region. Concerning the sagittal plane deformity, the constant tendency was not recognized

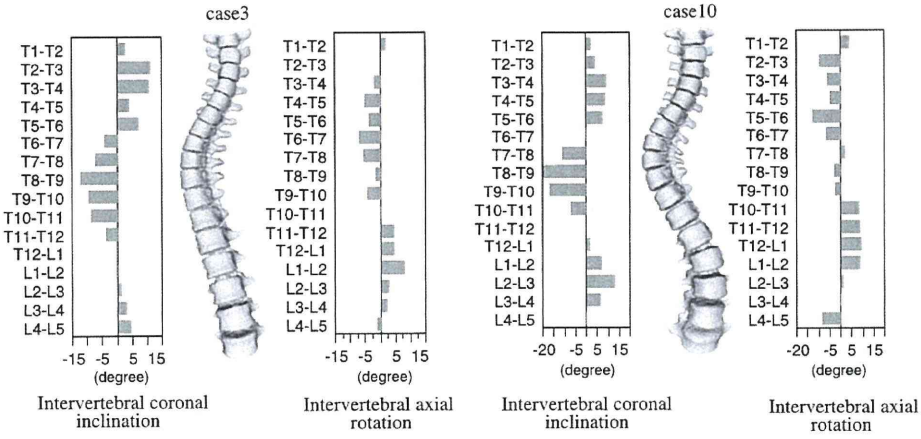

Fig. 4 Two representative cases. The bone models of both the thoracic and lumbar spine are shown in the *center*, and the *left sided graph* represents the intervertebral inclination angle in the coronal plane; the *right sided graph* represents the intervertebral rotational angle in the axial plane. *Left* case 3, *Right* case 10

in patients with AIS have been performed [8, 9, 21–23]. As morphometric studies, Parents et al. [21–23] created a 3D reconstruction of a large number of cadaveric bones, and compared normal vertebrae with the vertebrae of AIS. For example, vertebral wedging increased progressively toward the apex and pedicles located on the concavity were found to be significantly thinner than normal specimens [21–23]. In addition, the evaluation of global 3D correction between pre- and post-operative spinal 3D shape was also reported by Kadoury et al. [8, 9]. They reconstructed 3D models using bi-planar radiographs, and examined the difference among four operative methods. Steib et al. also performed 3D studies about the 3D change before and after surgical correction by in situ contouring technique using the reconstructed 3D models from bi-planar radiographs [6, 7, 16, 27]. However, these methods lacked accuracy since their method required only about 6–20 landmarks when reconstructing the bone models. Although an accurate assessment of 3D intervertebral deviation is crucial to the better surgical correction of the deformity, no detailed 3D study using an in vivo model of AIS has been reported.

Our results indicate the different deviation patterns between the intervertebral coronal plane deformity and intervertebral axial plane rotation. The intervertebral deformity in the coronal plane was larger near the apical region and smaller near the junctional region. Conversely, the intervertebral rotation in the axial plane was smaller near the apical region and larger near the junctional region. In 1994, Dubousset also showed that the intervertebral axial rotation reached its maximum at the extremities and its minimum at the apex [5]. However, the simple finite element models of only one case were used in the study and it is not known how to measure the intervertebral deviation [5]. Therefore, using the precise 3D evaluation method, we can show that the change in the intervertebral inclination angle in the coronal plane increased toward the apical region and decreased toward the junctional region, and that the converse tendency was noted for the axial intervertebral rotational angle in AIS patients for the first time.

There is a limitation in our method. The bone models were constructed from CT images taken in the supine position. Troell et al. [28] examined the radiographs of 287 girls with AIS and found that their mean Cobb angle, measured at standing position, was approximately 9° larger than that in the supine position, and the difference was 45° in the maximum. Yazici et al. [29] also showed that the average Cobb angle on a standing radiograph was approximately 16° larger than that in the supine position and they found that a rotational angle of 22.75° on the standing radiograph and 16.78° in the supine position. However, our results compared coronal with axial deviation under the same condition as supine. Though it is conceivable that the degree of the spinal deformity may be small in the supine position, it would appear that the features obtained from our study are not different from those obtained in the standing position.

The results in the present study can be applied to the surgical correction of AIS. The concave rod rotation maneuver, introduced by Cotrel and Dubousset, is generally concluded with derotation vertebral procedures. It's well accepted that rotation of precontoured concave rod (counter-clockwise) by alone has poor rotation improvement [1, 12–14, 17, 26]. Moreover, Kadoury et al. concluded that scoliosis also involves transverse plane rotation of the vertebrae in the opposite direction. In order to derotate the vertebrae, moments in the opposite sense should also be applied to the vertebrae [9]. According to our result, it might be easier to correct the rotation of each vertebra from the end vertebra to the apex using direct vertebral rotation technique.

Conclusion

We propose a new local coordinate system for deformed vertebrae of AIS. By using this coordinate system, the 3D intervertebral deviation in the coronal, axial and sagittal planes were measured. We found that the intervertebral deformity in the coronal plane was larger near the apical region and smaller near the junctional region. Conversely, the intervertebral rotation in the axial plane was smaller near the apical region and larger near the junctional region.

Conflict of interest None.

References

1. Asghar J, Samdani AF, Pahys JM, D'andrea LP, Guille JT, Clements DH, Betz RR (2009) Computed tomography evaluation of rotation correction in adolescent idiopathic scoliosis: a comparison of an all pedicle screw construct versus a hook-rod system. Spine 34:804–807
2. Benameur S, Mignotte M, Parent S, Labelle H, Skalli W, Guise J (2002) 3D biplanar statistical reconstruction of scoliotic vertebrae. Stud Health Technol Inform 91:281–285
3. Carpineta L, Labelle H (2003) Evidence of three-dimensional variability in scoliotic curves. Clin Orthop Relat Res 412:139–148
4. Cruickshank JL, Koike M, Dickson RA (1989) Curve patterns in idiopathic scoliosis. A clinical and radiographic study. J Bone Joint Surg [Br] 71:259–263
5. Dubousset J (1994) Three-dimensional analysis of the scoliotic deformity. In: Weinstein SL (ed) The pediatric Spine: Principles and Practices. Raven Press, New York, pp 479–496
6. Dumas R, Mitton D, Laporte S, Dubousset J, Steib JP, Lavaste F, Skalli W (2003) Explicit calibration method and specific device designed for stereoradiography. J Biomech 36:827–834
7. Dumas R, Steib JP, Mitton D, Lavaste F, Skalli W (2003) Three-dimensional quantitative segmental analysis of scoliosis corrected by the in situ contouring technique. Spine 28:1158–1162
8. Kadoury S, Cheriet F, Laporte C, Labelle H (2007) A versatile 3D reconstruction system of the spine and pelvis for clinical assessment of spinal deformities. Med Bio Eng Comput 45:591–602
9. Kadoury S, Cheriet F, Beauséjour M, Stokes IA, Parent S, Labelle H (2009) A three-dimensional retrospective analysis of the evolution of spinal instrumentation for the correction of adolescent idiopathic scoliosis. Eur Spine J 18:23–37
10. Kotwicki T, Napiontek M (2008) Intravertebral deformation in idiopathic scoliosis a transverse plane computer tomographic study. J Pediatr Orthop 28:225–229
11. King HA, Moe JH, Bradford DS, Winter RB (1983) The selection of fusion levels in thoracic idiopathic scoliosis. J Bone Joint Surg Am 65:1302–1313
12. Labelle H, Dansereau J, Bellefleur C, de Guise J, Rivard CH, Poitras B (1995) Peroperative three-dimensional correction of idiopathic scoliosis with the Cotrel–Dubousset procedure. Spine 15:1406–1409
13. Lenke LG, Bridwell KH, Baldus C, Blanke K, Schoenecker PL (1992) Cotrel–Dubousset instrumentation for adolescent idiopathic scoliosis. J Bone Joint Surg Am 74:1056–1067
14. Lenke LG, Bridwell KH, O'Brien MF, Baldus C, Blanke K (1994) Recognition and treatment of the proximal thoracic curve in adolescent idiopathic scoliosis with Cotrel–Dubousset instrumentation. Spine 15:1589–1597
15. Little DG, Sussman MD (1994) The Risser sign: a critical analysis. J Pediatr Orthop 14:569–575
16. Mitton D, Landry C, Véron S, Skalli W, Lavaste F, Guise JA (2000) 3D reconstruction method from biplanar radiography using non-stereocorresponding points and elastic deformable meshes. Med Biol Eng Comp 38:133–139
17. Moens P, Vanden Berqhe L, Fabry G, Bellemans J (1995) The Cortel–Dubousset device: prospective study on derotation. Rev Chir Orthop Reparatrice Appar Mot 81:428–432
18. Modi HN, Suh SW, Song HR, Lee SH, Yang JH (2008) Differential wedging vertebral body and intervertebral disc in thoracic and lumbar spine in adolescent idiopathic scoliosis—a cross sectional study in 150 patients. Scoliosis 3:11
19. Nash CL, Moe JH (1969) A study of vertebral rotation. J Bone Joint Surg Am 54:223–229
20. Oka K, Moritomo H, Murase T, Goto A, Sugamoto K, Yoshikawa H (2005) Patterns of carpal deformity in scaphoid nonunion: a 3-dimensional and quantitative analysis. J Hand Surg [Am] 30:1136–1144
21. Parent S, Labelle H, Skalli W, Latimer B, Guise J (2002) Morphometric analysis of anatomic scoliotic specimens. Spine 27:2305–2311
22. Parent S, Labelle H, Skalli W, Guise J (2004) Thoracic pedicle morphometry in vertebrae from scoliotic spines. Spine 29:239–248
23. Parent S, Labelle H, Skalli W, Guise J (2004) Vertebral wedging characteristic changes in scoliotic spines. Spine 29:E455–E462
24. Perdriolle R (1979) *La* scoliose: *Son* e'tude Tridimensionnelle. Ed. Maloine, Paris
25. Perdriolle R, Vidal J (1987) Morphology of scoliosis three-dimensional evolution. Orthopedics 10:909–915
26. Sawatzky BJ, Tredwell SJ, Jang SB, Black AH (1998) Effects of three-dimensional assessment on surgical correction and on hook strategies in multi-hook instrumentation for adolescent idiopathic scoliosis. Spine 23:201–205
27. Steib JP, Dumas R, Mitton D, Skalli W (2004) Surgical correction of scoliosis by in situ contouring: a detorsion analysis. Spine 29:193–199
28. Torell G, Nachemson A, Haderspeck-Grib K, Schultz A (1985) Standing and supine Cobb measures in girls with idiopathic scoliosis. Spine 10:425–427
29. Yazici M, Acaroglu ER, Alanay A, Deviren V, Cila A, Surat A (2001) Measurement of vertebral rotation in standing versus supine position in adolescent idiopathic scoliosis. J Pediatr Orthop 21:252–256

Three-dimensional kinematic estimation of mobile-bearing total knee arthroplasty from X-ray fluoroscopic images

Takaharu Yamazaki*[a], Kazuma Futai[b], Tetsuya Tomita[b], Yoshinobu Sato[c], Hideki Yoshikawa[d], Shinichi Tamura[a], Kazuomi Sugamoto[b]

[a] The Center for Advanced Medical Engineering and Informatics, Osaka University

[b] Division of Orthopaedic Biomaterial Science, Osaka University Graduate School of Medicine

[c] Department of Radiology, Osaka University Graduate School of Medicine

[d] Department of Orthopaedics, Osaka University Graduate School of Medicine

ABSTRACT

To achieve 3D kinematic analysis of total knee arthroplasty (TKA), 2D/3D registration techniques, which use X-ray fluoroscopic images and computer-aided design (CAD) model of the knee implant, have attracted attention in recent years. These techniques could provide information regarding the movement of radiopaque femoral and tibial components but could not provide information of radiolucent polyethylene insert, because the insert silhouette on X-ray image did not appear clearly. Therefore, it was difficult to obtain 3D kinemaitcs of polyethylene insert, particularly mobile-bearing insert that move on the tibial component. This study presents a technique and the accuracy for 3D kinematic analysis of mobile-bearing insert in TKA using X-ray fluoroscopy, and finally performs clinical applications. For a 3D pose estimation technique of the mobile-bearing insert in TKA using X-ray fluoroscopy, tantalum beads and CAD model with its beads are utilized, and the 3D pose of the insert model is estimated using a feature-based 2D/3D registration technique. In order to validate the accuracy of the present technique, experiments including computer simulation test were performed. The results showed the pose estimation accuracy was sufficient for analyzing mobile-bearing TKA kinematics (the RMS error: about 1.0 mm, 1.0 degree). In the clinical applications, seven patients with mobile-bearing TKA in deep knee bending motion were studied and analyzed. Consequently, present technique enables us to better understand mobile-bearing TKA kinematics, and this type of evaluation was thought to be helpful for improving implant design and optimizing TKA surgical techniques.

Keywords: Total knee arthroplasty, Mobile-bearing insert, 3D kinematics, Accuracy validation, X-ray fluoroscopy, 2D/3D registration technique, Clinical applications

1. INTRODUCTION

In orthopaedics, total knee arthroplasty (TKA) is an effective treatment for functional disability and arthritic knees in which articular cartilage is damaged. TKA implants generally consist of metallic femoral and tibial components and a polyethylene bearing insert between them (Figure 1). The polyethylene insert replaces the damaged cartilage of the tibial plateau and provides a low-friction surface for the metallic implant component.

Quantitative assessment of three-dimensional (3D) kinematics of TKA is highly important for evaluating the outcome of surgical procedures and for improving the implants design and clinical outcome. To achieve 3D kinematic analysis of TKA, 2D/3D registration techniques, which use X-ray fluoroscopic images and computer-aided design (CAD) model of the knee implant, have attracted attention in recent years [1-4]. These studies could provide information regarding the movement of radiopaque femoral and tibial components but could not provide information of radiolucent polyethylene insert, because the insert silhouette on X-ray image did not appear clearly. Therefore, it was difficult to obtain 3D kinemaitcs of polyethylene insert, particularly mobile-bearing insert that move on the tibial component.

Only a few studies have reported 3D kinematics of mobile-bearing insert in TKA using a fiducial markers technique based on X-ray images [5,6]. These studies are thought to be useful for 3D determination of the mobile-bearing insert kinematics. However, there is concern that the 3D pose estimation accuracy of the insert can be influenced by positional error of fiducial markers for the insert and projection number of makers on X-ray image. In previous studies, the pose estimation accuracy of the mobile-bearing insert has not been investigated, and therefore did not give assurance the same

Medical Imaging 2011: Image Processing, edited by Benoit M. Dawant, David R. Haynor,
Proc. of SPIE Vol. 7962, 79624B · © 2011 SPIE · CCC code: 1605-7422/11/$18 · doi: 10.1117/12.877815

degree of accuracy as femoral and tibial components. This study presents a technique and the accuracy for 3D kinematic analysis of mobile-bearing insert in TKA using X-ray fluoroscopy. The results of accuracy validation define the capabilities and limitations of 3D kinematic analysis of the insert. We also apply the technique to TKA patients during dynamic motion.

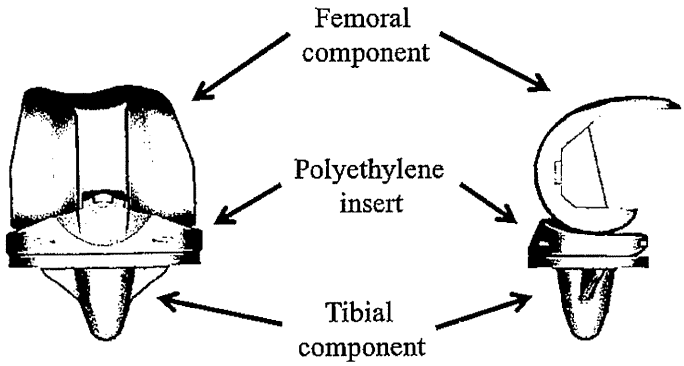

Figure 1. CAD models for femoral and tibial components and a polyethylene insert between them.

2. METHODS

2.1 Condition and requirement

To achieve 3D pose estimation of knee implants using X-ray fluoroscopy, it is necessary to know the parameters of the X-ray imaging system. The parameters of the imaging system are determined with a 3D calibration cube. The calibration cube has evenly spaced 217 metallic markers, which are employed as calibration markers. First, the calibration cube is placed in the viewing area of the imaging system and X-ray images are acquired. Next, because the X-ray images exhibit significant distortion introduced by image intensifiers, images are corrected with a non-linear distortion correction method. Finally, parameters of the imaging system (principal point and principal distance) are determined from 2D data (positions of the center of projected makers) on the corrected X-ray images and the known 3D data (positions and orientation) of the calibration cube with a non-linear calibration technique [7]. The principal point is the location on the image plane perpendicular to the incident X-ray, and the principal distance is the distance from the X-ray focus to the principal point.

In *vivo* knee motion after TKA was recorded as a series of digital X-ray images (1024x1024 pixels; 12 bits; 7.5 frames/sec) using a 12-inch digital image intensifier system (C-vision PRO-T, Shimadzu, Japan). Tests were typically performed using X-ray parameters of 70 kV, 400 mA and 1.2-2.0 ms duration, enabling nearly blur-free imaging of motion with higher per-frame exposure and image quality than in standard video-fluoroscopy.

2.2 Pose estimation of femoral and tibial components

For the 3D pose estimation of femoral and tibial components using X-ray fluoroscopy, a contour-based (feature-based) 2D/3D registration technique is utilized [2,4]. This technique uses implants silhouette contours on X-ray fluoroscopic images and CAD model of implants. The basic concept of this registration algorithm is that the 3D pose of a model can be determined by projecting rays from contour points in an image back to the X-ray focus, and noting that all of these rays are tangential to the model surface (Figure 2). The tangent condition therefore corresponds, in practice, to the minimum distance condition between the projection rays and the model surface. Then, a cost function E is defined as the sum of Euclidean distance d_i from point $\mathbf{q}_i$ on the projection rays (corresponding to the point p_i on the contours) to the closest point $\mathbf{s}_i$ on the CAD model surface.

$$E = \sum_{i=1}^{N} d_i^2 \tag{1}$$

The distance d_i is given by

$$d_i = \pm|\mathbf{q}_i - \mathbf{s}_i| \tag{2}$$

where $0 \leq i < N$ and N is the number of contour points. Negative values indicate rays that cross the model surface.

The 3D pose of the femoral and tibial component model is estimated by minimizing the cost function E (equation (1)) iteratively using a nonlinear optimization technique [8]. A good function for determining convergence of the 3D pose of the model is given by root mean square distance (RMSD):

$$\text{RMSD} = \sqrt{\sum_{i=0}^{N} d_i^2 \Big/ N} \tag{3}$$

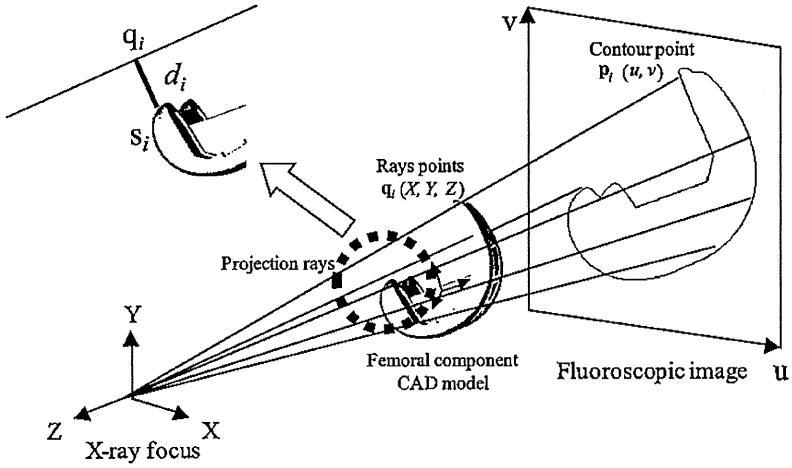

Figure 2. 3D pose estimation of the femoral component model from X-ray fluoroscopic images.

2.3 Pose estimation of mobile-bearing insert

To achieve 3D pose estimation of the mobile-bearing insert in TKA using X-ray fluoroscopy, tantalum beads are utilized. Because the polyethylene insert is transparent during fluoroscopy, four identical metallic tantalum beads are inserted at known positions of polyethylene insert using a specially designed insertion device during surgery. Holes of 2mm depth and small diameter are drilled, so that the 1mm tantalum beads are press fitted in the predefined non-critical areas of the insert. Therefore, CAD model of the polyethylene insert can be created with the four strategically placed beads (Figure 3). Because three points are required on a rigid body to define its 3D pose, at least three beads have to be located on fluoroscopic images. Hence, all metallic beads were offset as far as possible from adjacent beads in the sagittal and frontal planes of the polyethylene insert, insuring optimal determination of out-of-plane rotations. Figure 4 shows a representative beads silhouette on the X-ray fluoroscopic image.

To extract these beads silhouette markers from the X-ray image, a Gaussian Laplacian filter and Canny's edge detector were applied [9], and false edges including implants contours and noises detected were manually erased. After the identification of the beads on each fluoroscopic image in this way, the 3D pose of the insert model is estimated using a feature-based 2D/3D registration technique, which uses beads silhouette on fluoroscopic image and the corresponding insert CAD model with beads. A cost function is defined as described above equation (1), and likewise 3D pose estimation of the mobile-bearing insert is performed.

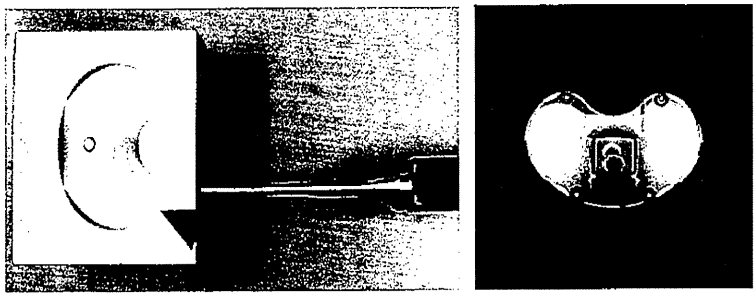

Figure 3. A specially designed insertion device (Left) and CAD model of the polyethylene insert with the four strategically placed beads (Right).

Figure 4. A representative beads X-ray image.

3. EXPERIMENTAL RUSULTS

3.1 Accuracy validation

In order to validate the accuracy of pose estimation for the mobile-bearing insert, two experiments were performed. In the first experiment, as a preliminary experiment, the repeatability of tantalum beads positions of polyethylene insert using a specially designed insertion device was investigated. Beads insertion of polyethylene insert using this device was repeated five times, beads positions of the five polyethylene inserts were accurately measured using high-resolution computed tomography. As a result of preliminary experiment, positional error of tantalum beads using this device was found to be 0.5 mm at most.

In the next experiment, based on the result of preliminary experiment, computer simulation test was performed. The positional errors within 0.5mm were randomly given for three or four strategically placed beads, and then synthetic tantalum beads silhouette images which had three or four beads were created for the insert in known typical orientations. In this study, a set of six synthetic tantalum beads silhouette images as shown in Figure 5 were used. The pose estimation errors of the insert were determined by comparing the estimated pose to the known pose.

The results of computer simulation test of pose estimation for the mobile-bearing insert are presented in Table 1. The root-mean-square errors (RMS errors) are given for each synthetic silhouette image. The RMS errors of all variables depended on the orientation pattern of the insert, while the difference of the error by beads projection number (three or four beads) for each orientation pattern (image 1,2 and image 3,4 and image 5,6) was small. The RMS errors of the five variables except for z (medial-lateral) translation were sufficiently smaller than 1.0 mm and 1.0 degree.

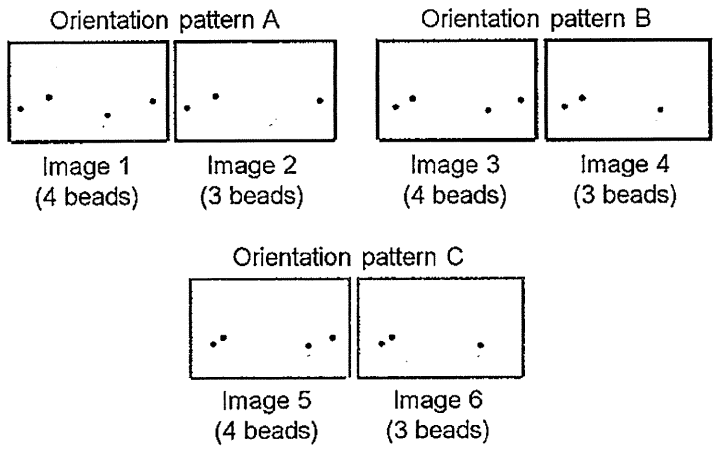

Figure 5. Synthetic tantalum beads silhouette images in typical orientations used for computer simulation test.

Table 1. Pose estimation errors for computer simulation test of the mobile-bearing insert.

RMS errors		Translation (mm)			Rotation (degrees)		
		x *posterior-anterior*	*y* *proximal-distal*	*z* *medial-lateral*	*x* *adduction-abduction*	*y* *internal-esternal*	*z* *extension-flexion*
Orientation pattern A	Image 1	0.20	0.17	0.83	0.13	0.27	0.22
	Image 2	0.30	0.48	0.99	0.14	0.30	0.22
Orientation pattern B	Image 3	0.43	0.14	0.96	0.18	0.47	0.32
	Image 4	0.41	0.39	1.02	0.23	0.43	0.34
Orientation pattern C	Image 5	0.52	0.67	1.48	0.49	0.53	0.47
	Image 6	0.65	0.84	1.63	0.51	0.58	0.45

3.2 Clinical applications

We finally applied the present technique to the mobile-bearing TKA patients during dynamic motion. The object of the study was explained to patients, and formal consent was obtained. Under fluoroscopic surveillance, dynamic movement in deep knee bending was conducted for total seven patients. Measurement values of each dynamic movement were described as the relative pose values of the femoral component with respect to the tibial component, and as that of the mobile-bearing insert with respect to the tibial component. For *in vivo* kinematic analysis, the relative pose of each knee implants model is determined by employing a three-axis Euler-angle system [10], and then the pose can be denoted by six variables, three translations and three rotations.

In the results of clinical applications, a representative image of the femoral and tibial CAD models overlaid on the X-ray image after 3D pose estimation, and an image of the mobile bearing insert estimated based on the metallic tantalum beads are shown in Figure 6. The sequence of relative poses in dynamic movement showed a smooth and reasonable physiologic pattern of motion, and the average range of motion for flexion-extension angle during the deep knee bending was 121.4 degree. In all seven patients, the femoral component rotated externally with respect to the tibial component during flexion, and the average external rotation range was 13.0 degree (Figure 7). Similarly, in all cases, the mobile-bearing insert also rotated externally with respect to the tibial component during flexion, and the average rotation range was 12.1 degree (Figure 8). In a few cases, the femoral component showed more external rotation than the mobile-bearing insert with respect to the tibial component during flexion, and the rotation angle was found to be about 5.0 degree at a maximum.

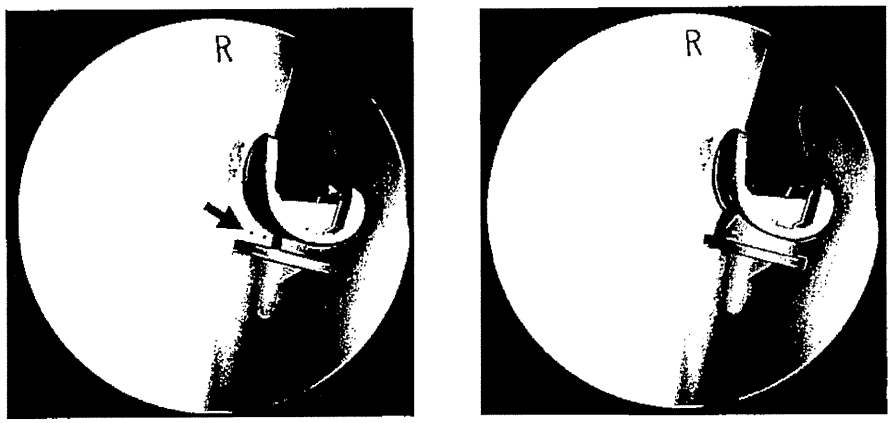

Figure 6. CAD model images from a representative TKA patient during deep knee bending. Femoral and tibial component models (Left) and mobile-bearing insert model (Right).

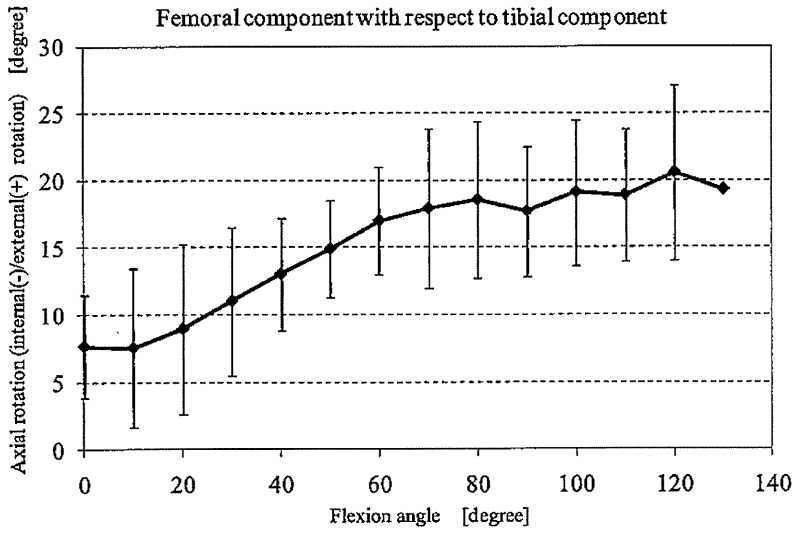

Figure 7. Axial rotation (internal/external rotation) of femoral component with respect to tibial component.

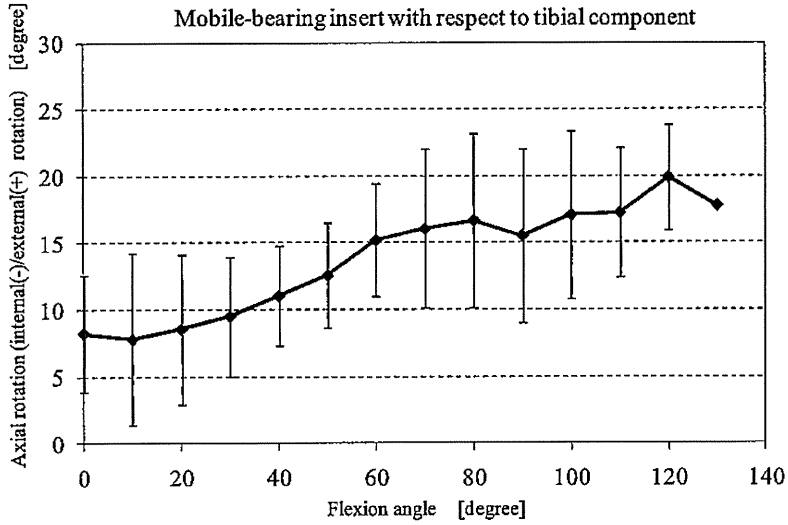

Figure 8. Axial rotation (internal/external rotation) of mobile-bearing insert with respect to tibial component.

4. DISCUSSION AND CONCLUSIONS

This study presented a procedure and the accuracy for 3D kinematic analysis of mobile-bearing insert in TKA using X-ray fluoroscopy, and finally performed clinical applications. Although it is difficult to obtain 3D kinemaitcs of the polyethylene mobile-bearing insert because the polyethylene insert is transparent during fluoroscopy, accurate measurement of the insert can be achieved by tracking previously inserted tantalum beads using a specially designed insertion device. Utilizing the inserted beads information (position and orientation) and present feature-based 2D/3D registration technique, the 3D pose estimation of the mobile-bearing insert was successfully performed.

The accuracy validation of the 3D pose estimation for the mobile-bearing insert was performed by two experiments, which has not been reported in previous studies. The accuracy of the pose estimation depended on the orientation pattern of the insert, and the errors of z (medial-lateral) translation were large due to use of single-plane X-ray image (Table 1). However, the difference of the error by beads projection number (three or four beads) was relatively small, and also even if positional errors within 0.5mm were given for three or four strategically placed beads, the accuracy of present technique was found to be sufficient for analyzing mobile-bearing TKA kinematics.

In the clinical applications, for seven TKA patients, relative axial rotations of three components (femoral component, tibial component, and mobile-bearing insert) were determined. The results showed that the mobile-bearing insert was primary rotating relative to the tibial component rather than the femoral component. Therefore, as the femoral component axially rotated, the mobile-bearing insert was rotating a similar magnitude in the same direction (Figure 7 and 8). While, in a few case, the femoral component showed more external rotation than the mobile-bearing insert with respect to the tibial component during flexion. This maybe indicates the femoral component was sliding on the mobile-bearing insert during flexion. Thus, present technique enables us to better understand mobile-bearing TKA kinematics. Consequently, this type of evaluation is thought to be helpful for improving implant design and optimizing TKA surgical techniques.

AKNOWLEDGMENTS

This study was supported in part by the Global COE Program "in silico medicine" at Osaka University.

REFERENCES

[1] Banks, S.A., Hodge, W.A., "Accurate measurement of three-dimensional knee replacement kinematics using single-plane fluoroscopy," IEEE Trans. Biomed. Eng. 43, 638-649 (1996).
[2] Zuffi, S., Leardini, A., Catani, F., Fantozzi, S., Cappello, A., "A model-based method for the reconstruction of total knee replacement kinematics," IEEE Trans. Meg. Imag. 18, 981-991 (1999).
[3] Mahfouz, M.R., Hoff, W.A., Komistek, R.D., Dennis, D.A., "A robust method for registration of three-dimensional knee implant models to two-dimensional fluoroscopy images," IEEE Trans. Meg. Imag. 22, 1561-1574 (2003).
[4] Yamazaki, T., Watanabe, T., Nakajima, Y., Sugamoto, K., Tomita, T., Yoshikawa, H., Tamura, S., "Improvement of depth position in 2-D/3-D registration of knee implants using single-plane fluoroscopy," IEEE Trans. Meg. Imag. 23, 602-612 (2004).
[5] Fantozzi, S., Leardini, A., Banks, S.A., Marcacci, M., Giannini, S., Cantani, F., "Dynamic in-vivo tibio-femoral and bearing motions in mobile bearing knee arthroplasty," Knee Surg. Sports Traumatol. Arthrosc. 12, 144-151 (2004).
[6] Komistek, R.D., Dennis, D.A., Mahfouz, M.R., Walker, S., Outten, J., "In vivo polyethylene bearing mobility is maintained in posterior stabilized total knee arthroplasty," Clin. Orthop. Relat. Res. 428, 207-213 (2004).
[7] Weng, J., Cohen, P., Herniou, M., "Camera calibration with distortion models and accuracy evaluation," IEEE Trans. Pattern Anal. Machine Intell. 14, 965-980 (1992).
[8] Luenberger, D.G., [Linear and Nonlinear Programming], Addison-Wesley, Facsimile Edition, Massachusetts (1984).
[9] Canny, J., "A Computational Approach to Edge Detection," IEEE Trans. Pattern Anal. Machine Intell. 8, 679-698 (1986).
[10] Grood, E.S., Suntay, W.J., "A joint coordinate system for the clinical description of three-dimensional motions: Application to the knee," J. Biomech. Eng. 105, 136-144 (1983).

幼児期発症の側彎変形に対するDSB(愛称プレーリーくん)による治療の試み(第一報)

The Dynamic Spinal Brace (Nick name : Prairie) used in the treatment for the infante with spinal deformity : A preliminary report.

大阪発達総合療育センター南大阪療育園
梶浦　一郎

大阪大学大学院　器官制御外科学
森口　悠

はじめに

幼児期（6歳未満）に発症する脊柱側弯変形には乳児期突発性側弯，先天性側弯，症候性側弯があるとされている．今回6歳未満でDynamic Spinal Braceを用いて治療を開始した症候性側弯22例について報告する．

DSB(愛称プレーリーくん)について

側弯の治療に用いる体幹装具は1958年にMilwaukee Braceが報告されて以来基本的概念は殆ど変らない．その装着の困難さから最近は殆どunderarm型が用いられている[4]．硬質の骨盤帯を基礎として強力な矯正力と固定により有効とされているが特に脳性麻痺児などの症候性側弯には装着困難な例が多い．そこで我々は固定ではなく動的な矯正力と体幹の立ち直り機能を促進する装具を新たに作製した．支柱はポリカーボネイト製で，弾力を有して上部胸郭と骨盤外側面（腸骨稜ではない）とハンプ押えによる三点支持の原理により弾力的な矯正力の動くことを目的としたものであり，その基本理念から動的体幹装具(Dynamic Spinal Brace）と名付けた[3]．腸骨稜を避けることにより，同部に多く見られた皮膚障害（痛み，発赤）は殆ど無くなったが，装着中に装具が回旋することが起こりやすい欠点が判明した（DSB Ⅱ型）（図1）．そこで両大臀筋部を対称的に押える翼を加えることにより，安定して装着できるようになった（DSB Ⅲ型）．

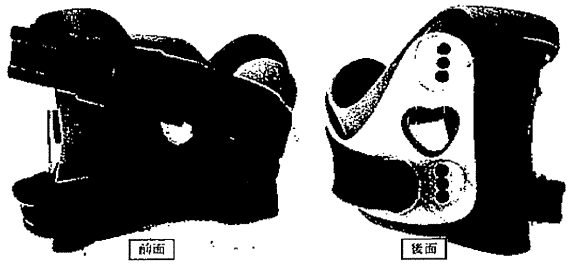

図1．DSB Ⅱ型の特徴
- 弾性のある3点支持，“固定”ではなく“たわみ”を利用する
- 装着時間は“状態に応じて徐々に延長する”
- 接触面積が少なく，軽量である．

特許番号　4747327

症例の概要

年齢は1歳～5歳（平均2.8歳）であり男

Key words：幼児期（Infante），症候性側弯（symptomatic Scoliosis），DSB（Dynamic spinal Brace）．